

# APERIODIC MAGNETIC TURBULENCE PRODUCED BY RELATIVISTIC ION BEAMS

JACEK NIEMIEC

Instytut Fizyki Jądrowej PAN, ul. Radzikowskiego 152, 31-342 Kraków, Poland

MARTIN POHL

Department of Physics and Astronomy, Iowa State University, Ames, IA 50011

ANTOINE BRET

ETSI Industriales, Universidad de Castilla - La Mancha, 13071 Ciudad Real, Spain

AND

THOMAS STROMAN

Department of Physics and Astronomy, Iowa State University, Ames, IA 50011

*Draft version November 8, 2018*

## ABSTRACT

Magnetic-field generation by a relativistic ion beam propagating through an electron-ion plasma along a homogeneous magnetic field is investigated with 2.5D high-resolution particle-in-cell (PIC) simulations. The studies test predictions of a strong amplification of short-wavelength modes of magnetic turbulence upstream of nonrelativistic and relativistic parallel shocks associated with supernova remnants, jets of active galactic nuclei, and gamma-ray bursts. We find good agreement in the properties of the turbulence observed in our simulations compared with the dispersion relation calculated for linear waves with arbitrary orientation of  $\vec{k}$ . Depending on the parameters, the backreaction on the ion beam leads to filamentation of the ambient plasma and the beam, which in turn influences the properties of the magnetic turbulence. For mildly- and ultra-relativistic beams, the instability saturates at field amplitudes a few times larger than the homogeneous magnetic field strength. This result matches our recent studies of nonrelativistically drifting, hot cosmic-ray particles upstream of supernova-remnant shocks which indicated only a moderate magnetic-field amplification by nonresonant instabilities. We also demonstrate that the aperiodic turbulence generated by the beam can provide efficient particle scattering with a rate compatible with Bohm diffusion. Representing the ion beam as a constant external current, i.e. excluding a backreaction of the magnetic turbulence on the beam, we observe non-resonant parallel modes with wavelength and growth rate as predicted by analytic calculations. In this unrealistic setup the magnetic field is amplified to amplitudes far exceeding the homogeneous field, as observed in recent MHD and PIC simulations.

*Subject headings:* acceleration of particles, cosmic rays, gamma rays: bursts, methods: numerical, shock waves, turbulence

## 1. INTRODUCTION

Collisionless shocks are the acceleration sites of energetic particles responsible for high-energy emission of astrophysical objects and contributing to the flux of cosmic rays detected at Earth. Nonthermal particle populations at nonrelativistic shocks of supernova remnants (SNRs) are believed to be generated by diffusive shock acceleration (DSA). The particle spectra thus produced indeed agree well with those deduced from radio-to-X-ray electron synchrotron emission of SNRs (Reynolds 2008). The high efficiency of the DSA mechanism together with considerations of the global energetics of a supernova explosion make the forward shocks of shell-type SNRs the prime candidates for the sources of Galactic cosmic rays (CRs). Nonthermal power-law particle spectra attributed to relativistic electrons are also inferred from modeling the electromagnetic emission from astrophysical sources harboring relativistic shock waves, such as jets of active galactic nuclei (AGN) and gamma-ray

bursts (GRBs) (Mészáros 2002).

Efficient particle acceleration at shocks invariably requires a continuous excitation of magnetic turbulence in the upstream region, which serves as a scattering medium to confine the energetic particles to the shock region for further acceleration (Malkov & Diamond 2001). Turbulent magnetic fields of amplitude much larger than the homogeneous interstellar field are needed upstream of SNR shocks to account for protons of energies up to and beyond the "knee" at  $10^{15}$  eV in the cosmic-ray spectrum. Recent X-ray observations of several young SNRs give evidence that indeed highly amplified fields exist downstream of SNR forward shocks (see Reynolds (2008), and references therein). Downstream of ultrarelativistic GRB external shocks the magnetic fields must also be amplified orders of magnitude beyond shock-compression levels to explain GRB afterglow spectra and light curves. Even in the preshock medium magnetic fields of milligauss strengths are required to account for the observed X-ray afterglows (Li & Waxman 2006).

A plausible scenario for magnetic-field generation as

sumes that cosmic ray particles accelerated at the shock drift as an ensemble relative to the upstream plasma and trigger a variety of instabilities that may lead to the growth of a turbulent field component (Bell & Lucek 2001; Bell 2004). The distribution function of the cosmic rays is shaped by the scattering rate in the self-excited field upstream, thus forcing a nonlinear relationship between the upstream plasma, the energetic particles, and small-scale electromagnetic fields. The upstream field would subsequently be advected and compressed downstream of the shock and possibly further amplified by fluid instabilities in the downstream plasma (Giacalone & Jokipii 2007; Zirakashvili & Ptuskin 2008; Couch et al. 2008). While a full modeling of the upstream region is elusive to date, simulations of turbulence build-up using prescribed distribution functions for the upstream plasma and the cosmic rays can be invaluable tools for the study of the saturation processes and levels, as well as the backreaction of the evolved turbulence on the particles. The system in which a population of cosmic rays slowly drifts relative to the upstream plasma has been studied with MHD simulations, which represented cosmic rays with a constant external current (Bell 2004, 2005; Zirakashvili et al. 2008; Reville et al. 2008) and with first-principles particle-in-cell (PIC) simulations assuming a constant cosmic-ray current (Ohira et al. 2009) or including the full dynamics of the energetic particles (Niemiec et al. 2008; Stroman et al. 2009; Riquelme & Spitkovsky 2009). They confirmed the quasi-linear predictions by Bell (2004), who showed that for the parameters of young SNRs, magnetic turbulence would appear in a form of nonresonant, circularly polarized, and aperiodic transverse waves. Numerical simulations analyzing the nonlinear evolution of the system found that the turbulence growth eventually saturates, but the exact saturation levels differ between the approaches, the full PIC simulations typically yielding considerably lower field amplitudes than MHD studies with constant CR currents.

Here we report kinetic (PIC) simulations of the interaction between the far-upstream plasma and a cold dilute relativistic beam of particles streaming along a homogeneous background magnetic field. We assume that the beam is composed of cosmic-ray ions, and the current and charge carried by the beam is balanced by electrons of the background medium. The situation is relevant to the upstream region of both relativistic and nonrelativistic shocks undergoing efficient particle acceleration. In a SNR shock environment, it applies to the most energetic cosmic rays accelerated at the shock which stream far upstream of the free-escape boundary. In this case, a predominantly ionic cosmic-ray component results from the character of injection processes at nonrelativistic shocks. Upstream of relativistic shocks of GRBs and AGN, distributions of particles accelerated in a wide energy range are highly anisotropic. This is because particles and the shock move close to the speed of light, and a deflection of a particle trajectory by an angle greater than  $\Gamma_{sh}^{-1}$  allows the shock to overtake the particle. Therefore, in the upstream rest frame the non-thermal particles are highly beamed and their transverse momenta are a factor of  $\Gamma_{sh}^{-1}$  smaller than the momenta along the shock direction. We approximate this sit-

uation by assuming that the CR beam is cold. This assumption better holds for the freshly accelerated particles in the far-upstream region, whose transverse momenta are much smaller than  $\Gamma_{sh}^{-1}$  times the parallel momentum; the highest-energy particles escape from the precursor and therefore have an anisotropic distribution in the shock rest frame, which is further enhanced by the shock curvature. Some instabilities, e.g. filamentation, depend sensitively on the transverse temperature of the CR beam, and care must be exercised in extrapolating our simulation results to situations in which the CR-beam properties are somewhere between those of the cold beam studied here and the very hot, but slow beam investigated earlier (Niemiec et al. 2008; Stroman et al. 2009; Riquelme & Spitkovsky 2009). However, PIC simulations of relativistic shocks in electron-ion plasmas suggest that filamentation indeed occurs only far upstream of the shock (Spitkovsky 2008a; 2008b; see also Medvedev & Zakutnyaya 2009), and it is generated by a warm ( $p_{\perp} \lesssim p_{\parallel}/\Gamma_{sh}$ ) ion beam. We may therefore expect that our assumption of a cold CR beam remains a valid approximation for systems with warm CR beams. Furthermore, our setup applies to the cosmic-ray ions whose energies are larger than the upper limit on the energy of electrons accelerated by the shock, which is imposed by radiative energy losses (e.g. Li & Waxman 2006). The highly energetic ions will thus reach farther upstream than the CR electrons and the return current will be provided by the ambient electrons.

Note that the applicability of the system under study to relativistic astrophysical sources relies on the ability of relativistic shocks to accelerate particles to very high energies. Although the first-order Fermi process at such shocks is widely considered to be the source of cosmic rays, recent studies in the test particle approximation (Niemiec & Ostrowski 2006; Niemiec et al. 2006; Lemoine et al. 2006) and using PIC simulations (Sironi & Spitkovsky 2009) show that this mechanism can operate only in quasi-parallel or weakly magnetized shocks. If the GRB or AGN outflows are strongly magnetized /quasi-perpendicular, some other processes must be responsible for particle acceleration (e.g., magnetic reconnection), and our results do not apply.

It is known from studying non-relativistic beams in interplanetary space that a competition arises between resonant and nonresonant modes, which exert different backreactions on the beam (Winske & Leroy 1984). For the case of a monoenergetic, unidirectional distribution of streaming cosmic rays, the rates for the resonant growth of Alfvénic (Pohl & Schlickeiser 2000) and electrostatic (Pohl et al. 2002) turbulence have been derived using quasilinear theory. Based on an analytical treatment, Reville et al. (2006) found that also in this case nonresonant, purely growing modes may be expected to be significantly faster, although the growth rate falls off with the temperature of the background medium. Application of this mechanism to the external GRB shocks was phenomenologically studied by Milosavljević & Nakar (2006), who concluded that CR-driven turbulence may account for the levels of amplified magnetic fields inferred from these sources. We have performed a series of two-dimensional simulations for this setup to explore the relationship between this instabil-

ity and that found for drifting cosmic rays, and to determine the mutual backreaction between the magnetic turbulence and the CR beam. The interaction of a cold relativistic ion beam is studied in the limit of a magnetized background plasma, for which the results of the analytical calculations of Reville et al. (2006) apply.

The simulation setup is described §2 and the results of the linear kinetic analysis of the system are presented in §3. In §4 the simulation results are presented. The differences in the properties of the system between the runs representing the CR beam with a constant external current and the fully kinetic simulations are discussed in §4.1 and §4.2. The detailed properties of the magnetic turbulence and the evolution of particle phase-space distributions are then presented in §4.3 based on the results for mildly relativistic ion beams. We conclude with a summary and discussion in §5.

## 2. SIMULATION SETUP

The code used in this study is a 2.5D (2D3V) version of the relativistic electromagnetic particle code TRISTAN with MPI-based parallelization (Buneman 1993; Niemiec et al. 2008). In the simulations a cold, relativistic, and monoenergetic cosmic-ray ion beam with Lorentz factor  $\gamma_{CR}$  (velocity  $v_{CR}$ ) and number density  $N_{CR}$  streams along a homogeneous magnetic field  $B_{\parallel 0}$  relative to the ambient electron-ion plasma. The ions of the ambient medium have a thermal distribution with number density  $N_i$ , in thermal equilibrium with the electrons. The electron population with density  $N_e = N_i + N_{CR}$  contains the excess electrons required to provide charge-neutrality and drifts with  $v_d = v_{CR}N_{CR}/N_e$  with respect to the background ions, so it provides a return current balancing the current carried by the ion beam. We have explored the system in the limit of a magnetized background plasma,  $\omega \ll \Omega_i$  (see (Reville et al. 2006)). Specifically, we assumed  $\gamma_{max}/\Omega_i = 0.2$ , where

$$\gamma_{max} = \Im\omega \approx \frac{1}{2} \frac{v_{CR} N_{CR}}{v_A N_i} \Omega_i \quad (1)$$

is the growth rate of the most unstable nonresonant mode,  $\Omega_i$  is the ion gyrofrequency, and  $v_A = [B_{\parallel 0}^2/\mu_0(N_e m_e + N_i m_i)]^{1/2}$  is the plasma Alfvén velocity. The relativistic cosmic-ray populations represent very dilute ion beams which we study with density ratios  $N_i/N_{CR} = 50$  and 125, and Alfvén velocities  $v_A = c/20$  and  $v_A = c/50$ , respectively (for which the ratio  $\omega_{pe}/\Omega_e = 4.4$  and 11.0, respectively). The simulations have been performed for the case of an ultrarelativistic beam with  $\gamma_{CR} = 300$  and a slower beam with  $\gamma_{CR} = 20$ . We have also studied the case in which the beam is represented by a constant uniform external current, so that the backreaction of the magnetic turbulence on the cosmic-ray beam is suppressed. The parameters of all simulation runs described here are summarized in Table 1.

To ensure the numerical accuracy of our simulations, we use a total of 16 particles per cell, and we apply the splitting method for the beam particles. The density ratio between simulated cosmic-ray and ambient particles on the grid is 1/3, and weights are applied to each beam particle to match the desired  $N_{CR}/N_i$ . The same weights are used for the excess electrons  $\delta N_e = N_e - N_i = N_{CR}$ ,

and thus each ion particle can be initialized at the same location as the corresponding electron for the identically zero initial charge density. The electron skindepth  $\lambda_{se} = c/\omega_{pe} = 4\Delta$ , where  $\omega_{pe} = (N_e e^2/m_e \epsilon_0)^{1/2}$  is the electron plasma frequency and  $\Delta$  is the grid cell size. We further assume a reduced ion-electron mass ratio  $m_i/m_e = 20$ . This choice allows us to clearly separate the plasma and turbulence scales and yet use a computational box that can contain several wavelengths of the most unstable mode

$$\lambda_{max} \approx 2\pi(\gamma_{max}/\Omega_i)^{-1}\lambda_{si}, \quad (2)$$

where  $\lambda_{si}$  is the ion skindepth. As the results of our linear analysis of §3 show, the one-dimensional dispersion relations obtained by Reville et al. (2006) capture the physical properties of the system, provided the Lorentz factor of the ion beam is very large or a constant external current is applied. In this study we perform simulations for an ultrarelativistic beam and for the case of a constant external cosmic-ray current to cross-check those results as well as the validity of our approach. For these runs we use smaller computational grids:  $(L_x, L_y) = (7.4\lambda_{max}, 5.7\lambda_{max})$  for runs A and D, and  $(L_x, L_y) = (4.6\lambda_{max}, 3.3\lambda_{max})$  for run B. Larger grids with  $(L_x, L_y) = (10.2\lambda_{max}, 7.4\lambda_{max})$  are used to investigate the systems with mildly relativistic cosmic-ray beams, which have not been studied with PIC simulations before. Cosmic-ray beam ions move in the  $-x$ -direction, antiparallel to the homogeneous magnetic field  $B_{\parallel 0}$ . Periodic boundary conditions are assumed for all boundaries. In all simulations the time step is  $\delta t = 0.1125/\omega_{pe}$ , and the inverse maximum growth rate of the nonresonant modes  $\gamma_{max}^{-1} = 3975\delta t$  for runs A–C and  $9938\delta t$  for runs D and E.

Our previous work on similar systems as well as additional test runs performed for the current study ensures that our results are not affected by a particular choice of simulation parameters, e.g., electron-ion mass ratio, number of particles per cell, or the electron skindepth. The validity of two-dimensional simulations in capturing the essential physics has been demonstrated in Niemiec et al. (2008).

## 3. LINEAR ANALYSIS

The growth rate and wavelength of the most unstable purely-growing nonresonant mode given by equations 1 and 2 were obtained by Bell (2004) and Reville et al. (2006) using linear kinetic analysis in the limit of a cold ambient plasma and only for wavevectors  $k_{\parallel}$  parallel to  $B_{\parallel 0}$ . We have numerically calculated the growth rates for arbitrary orientation of the wavevector,  $\vec{k}$ , in the zero-temperature limit (for details of the calculations see, e.g., (Bret 2009)). In Figure 1 we show the growth rates in the reduced wavevector space  $(Z_{\parallel}, Z_{\perp})$ ,  $Z_i = k_i v_{CR}/\omega_{pe}$ , that is contained in our simulation box, for beams moving along a homogeneous magnetic field of strength given by the Alfvén velocity of  $v_A = c/20$ . In each case the dominant unstable mode is the electrostatic Buneman mode between background ions and drifting electrons ( $Z_{\parallel} \gtrsim 2$ ). The growth rate of this mode is about  $10^2$  times larger, and its wavelength about  $1.25 \times 10^3$  shorter than that of the nonresonant mode (see Eqs. 1 and 2). Our simulations do not fully resolve this mode, because

the wavelength of maximum growth corresponds to half a cell ( $Z_{\parallel} \approx 55$ ) on our computational grid, and we are able to see longer wavelength modes only with somewhat smaller growth rates. However, the Buneman instability is very sensitive to thermal effects and should saturate if the thermal velocity of ambient particles becomes comparable to their relative drift velocity. The initial electron thermal velocity in the simulations is thus set to values  $v_{e,th} \lesssim v_d$  to ensure the quick saturation and dissipation of this unstable mode. Note that such plasma parameters well reproduce the real conditions in astrophysical objects, and the Buneman mode will be relevant only if the beam density is high, because then  $v_d$  will be high as well.

The nonresonant mode, which we are chiefly interested in, is visible at  $Z_{\perp} < 0.1$  and shows a broad peak centered at  $Z_{\parallel} \approx 0.05$ , corresponding to the estimate given by Eq. 2. However, if the CR beams are treated fully kinetically ( $\gamma_{CR} = 300$  and  $20$  – Fig. 1b and Fig. 1c, respectively), the nonresonant mode is not dominant even in the limited wavevector space covered in our simulations. In fact, the strongest growth occurs for  $0.3 < Z_{\perp} < 1$ , almost independent of  $Z_{\parallel}$ . The very peaked growth at  $Z_{\parallel} \approx 1$  pertains to the Buneman instability between relativistic ion beam and ambient electrons. The growth at smaller  $Z_{\parallel}$  represents the filamentation of the ambient plasma and the ion beam. The appearance of these fast-growing modes modifies the system, and one should expect that the properties of the nonresonant mode emerging in the nonlinear stage differ from those predicted in the analytical calculations by Reville et al. (2006). This is in fact what is observed in our simulations. It should be noted, though, that for warm CR beams filamentation might be suppressed, and therefore may not play a role in the precursor region close to the shock.

Note that the growth rates as shown in Figure 1 depend on the parameters of the system under study. In particular, for ultrarelativistic beams (Fig. 1b) the growth rate for the filamentation modes is much smaller than for  $\gamma_{CR} = 20$ . Hence, for  $\gamma_{CR} \gtrsim 100$  we primarily have a competition between the nonresonant mode and the Buneman modes. If we replace the ion beam by an constant external current (which somewhat corresponds to  $\gamma \gg 1$ , Fig. 1a), then the ambient electrons do not interact with the ion beam, and a Buneman instability is not excited. The evolution of the system is then artificially dominated by the nonresonant instability (Ohira et al. 2009).

## 4. SIMULATION RESULTS

### 4.1. Simulations with Constant Cosmic-Ray Current

The temporal evolution of the energy density in the transverse magnetic-field component is shown in Figure 2a. If the backreaction on the cosmic rays is suppressed, i.e., a constant uniform external current is applied, then a purely-growing parallel mode of magnetic turbulence appears in the plasma. Its growth rate ( $\gamma \approx 0.8\gamma_{max}$  for the two cases with  $v_A = c/20$  and  $c/50$ , run A and D, respectively) and wavelength (dashed line in Fig. 2b) agree well with those predicted by quasi-linear analytical calculations. The mode represents a purely magnetic, circularly polarized, and aperiodic transverse wave. The interactions of the magnetic

turbulence with the plasma are predominantly related to the return current carried by the ambient electrons,  $\vec{j}_{ret}$ . The  $\vec{j}_{ret} \times \delta B_{\perp}$  force induces motions and turbulence in the background plasma, which in the later stages cause the turbulence to turn nearly isotropic and highly nonlinear. As in the case of drifting cosmic rays (Niemiec et al. 2008) and nonrelativistic beams (Winske & Leroy 1984), the saturation of the magnetic-field growth proceeds via bulk acceleration and occurs when the bulk velocity of the background plasma approaches the cosmic-ray ion beam speed (see §4.3.2.). Note that current and charge balance is still observed if the cosmic-ray current is chosen constant, and the background plasma is charged by adding extra electrons to compensate for the charge of the cosmic rays. The plasma thus "knows" the cosmic-ray drift speed as that at which the plasma electrons no longer stream relative to the plasma ions to carry the return current. The nonlinear amplitude of the field perturbations is slightly larger for smaller Alfvén velocity, in agreement with Riquelme & Spitkovsky (2009). However, the magnetic-field amplitudes become comparable at the end of both runs, and reach  $\delta B_{\perp}/B_{\parallel 0} \simeq 25$ , which is close to the maximum obtained with MHD simulations (Bell 2004, 2005; Zirakashvili et al. 2008) and other PIC simulations (Ohira et al. 2009), in which the cosmic rays were also represented by a constant current.

We will now describe the behavior of the system including the response of the relativistic cosmic-ray ion beam.

### 4.2. Fully Kinetic Simulations

If the cosmic rays are treated fully kinetically, the dynamics of the system changes. The interaction of the ion beam with the plasma quickly leads to plasma and beam filamentation which is modified by a Buneman instability between the ion beam and plasma electrons. The Buneman beam-electron interactions produce mainly electrostatic, slightly oblique turbulence whose wavelength parallel to the direction of the beam is in very good agreement with the predictions of our linear analysis, which gives  $\lambda = 2\pi(v_{CR}/c)\lambda_{se} \sim 25\Delta$  (§3). The mode grows very fast, causing density fluctuations in the beam and electron plasma. However, in the simulations its amplitude quickly saturates and is subsequently kept at a moderate level. These features are in agreement with the known properties of the Buneman modes (see, e.g., Dieckmann et al. (2007) for a detailed discussion of the nonlinear evolution and saturation mechanism of the Buneman instability). The Buneman mode dissipates only after filamentation and nonresonant modes have strongly backreacted on the ion beam in the nonlinear stage.

#### 4.2.1. Ultrarelativistic Beams

The properties of the magnetic turbulence depend on the Lorentz factor of the beam. For an ultrarelativistic beam with  $\gamma_{CR} = 300$  (run B; dotted lines in Fig. 2), the filamentation is weak and the parallel nonresonant mode appears with the theoretically predicted wavelength. Its growth rate is initially  $\gamma \approx 0.94\gamma_{max}$  and decreases during the nonlinear evolution. As one can see in Figure 2a, the peak amplitude of the magnetic-field perturbations,  $\delta B_{\perp}/B_{\parallel 0} \simeq 9$ , is close to that obtained with constant external current (run A; solid line) at the onset of the satu-

ration of the turbulence growth ( $t \sim 15\gamma_{max}^{-1}$ ). It appears that in this phase the high beam Lorentz factor provides sufficient stiffness to the ion beam that its backreaction is suppressed, rendering the system response similar to that for a constant external current. The similarity ends when the saturation kicks in, though. The subsequent dissipation of the turbulence in the run with  $\gamma_{CR} = 300$  is much stronger than in the case of a constant external current, which places in doubt the accuracy of simulations that use a constant external current to describe the highly nonlinear phases in the evolution of the system.

#### 4.2.2. Mildly Relativistic Beams

Results for a system with a mildly relativistic beam with  $\gamma_{CR} = 20$ , and for  $v_A = c/20$  (run C) and  $c/50$  (run E), are presented in Figure 2a with dash-dotted and long-dashed lines, respectively. As our linear analysis of §3 shows, the filamentation modes at perpendicular wavevectors  $k_{\perp} \approx 1/\lambda_{se}$  are strong in this case. They cause filamentation in the ambient plasma and the ion beam, before the nonresonant parallel modes have emerged. As one can see in Figure 2, these modes do not lead to magnetic-field perturbations of significant amplitude. Nevertheless, their action on the ambient plasma changes its properties, which considerably influences the characteristics of the purely-growing parallel modes. The nonresonant modes appear in a broad range of wavelengths around  $\lambda_{max}$  (Fig. 2b), and the growth rate of the magnetic-field perturbations is only  $\sim 0.4\gamma_{max}$ . The backreaction of the turbulence on the system further enhances the filamentation in the beam and the plasma, and leads to the saturation and dissipation of the magnetic turbulence at a level a few times the homogeneous magnetic field strength. The peak amplitudes for the two cases with  $v_A = c/20$  and  $c/50$  are  $\delta B_{\perp}/B_{\parallel 0} \simeq 4.7$  and  $\delta B_{\perp}/B_{\parallel 0} \simeq 7.5$ , respectively, showing that instabilities operating in a less-magnetized medium provide a stronger field amplification. It is unclear whether the modification of the parallel mode arises specifically from filamentation or from any type of perpendicular, small-scale density fluctuations, including preexisting turbulence. We can therefore not reliably predict the behavior of a system containing a warm cosmic-ray beam, for example the denser parts of a cosmic-ray precursor to an astrophysical shock.

### 4.3. Aperiodic Magnetic Turbulence Produced by Mildly Relativistic Beams

#### 4.3.1. Spectral Properties of the Turbulence

The characteristic features of magnetic turbulence in a system containing a mildly relativistic cosmic-ray beam are detailed in Figures 3, 4, and 5 for the run with  $\gamma_{CR} = 20$  and  $v_A = c/20$  (run C). The temporal evolution of the magnetic and electric field average energy densities is shown in Figure 3. Figure 4 presents Fourier power spectra of the perpendicular magnetic-field component  $B_z$  for  $t\gamma_{max} = 2, 5$ , and 8 in two-dimensional reduced wavevector space ( $Z_{\parallel}, Z_{\perp}$ ). Figure 5 shows snapshots of the time evolution of the electron and cosmic-ray ion density, and the structure in the  $B_z$  magnetic-field component.

The initial filamentation in the ambient plasma grows quickly in spatial scale by merging of adjacent filaments,

which can be clearly seen in  $E_x$  and  $E_y$ , and also in the  $B_z$  field components shown in Figure 4. Because the Buneman instability between the ion beam and the plasma electrons is slightly oblique (see Fig. 1c), hence not purely electrostatic, it is visible in magnetic-field Fourier spectra as a feature at  $Z_{\parallel} \approx 1$  (Fig. 4). The corresponding strong short-scale modulations in the densities of ambient electrons and the ion beam can be seen in Figure 5a-b and Figure 5d-e. The nonresonant parallel modes of magnetic turbulence emerge in a medium already strongly modified by filamentation. They appear in a range  $0.02 \lesssim Z_{\parallel} \lesssim 0.1$  around the theoretically predicted  $Z_{\parallel}(\lambda_{max}) \simeq 0.08$  and quickly grow in wavelength (see Figs. 4b-c, 5c, and 5f). The influence of the nonresonant modes is stronger on the filamentation in the slowly drifting ambient plasma than that in the relativistic ion beam. In essence, ambient plasma filaments become vertically tilted (Fig. 5d), which leads to even stronger plasma filamentation. The lack of spatial correlation between filaments in the ambient plasma and the beam results in a local charge imbalance and the build-up of charge-separation electric fields, which, together with electric fields induced by the Buneman instability, dominate the turbulent electromagnetic energy content of the system in the initial stage (Fig. 3). During the nonlinear stage ( $t \gtrsim 8\gamma_{max}^{-1}$ ) the enhanced filamentation leads to the generation of stronger turbulence in the  $B_z$  component of the magnetic field with perpendicular wavevectors,  $k_y$ , which disrupts the structure of the parallel magnetic modes. This interaction between filamentary and nonresonant modes is visible in Figure 5f and in the Fourier spectrum in Figure 4c.

As one can see in Figures 5g-i, the strongly amplified magnetic field starts to backreact on the cosmic-ray beam in the later stage of the system evolution. Cosmic-ray filaments become tilted and eventually disrupted. This is accompanied by turbulent ambient plasma motions and results in highly nonlinear and nearly isotropic magnetic turbulence. The characteristics of the turbulence in its post-saturated state are thus similar to those observed in simulations of nonrelativistically drifting hot cosmic-rays in the precursor to SNR shocks.

#### 4.3.2. Particle Phase-Space Distributions

The effects of the backreaction of the magnetic turbulence on the particles are presented in Figures 6, 7, and 8. The average (bulk) velocities of all particle species converge in the nonlinear stage, when the magnetic-field growth saturates (at  $t \approx 15\gamma_{max}^{-1}$  for runs A and C in Fig. 6). While the relative drift between the plasma and the cosmic-ray beam disappears in all our simulations, the mechanism by which that is achieved differs between runs which suppress the cosmic-ray backreaction and fully kinetic runs.

In the fully kinetic simulations (solid line in Fig. 6), the cosmic-ray beam slows down considerably, and the ambient plasma accelerates up to  $\sim -0.2c$ . This behavior is similar to the results of Winske & Leroy (1984) for nonrelativistic dilute ion beams interacting with ambient plasma via nonresonant modes, which showed that the energy of the decelerating beam is transferred in approximately equal parts to the ambient ions and the magnetic field, in accordance to the predictions of quasi-linear the-

ory. The simulation results of Winske & Leroy (1984) were obtained with a one-dimensional hybrid model that treats electrons as a massless fluid, with which one cannot observe filamentation modes, and the associated electron heating is artificially suppressed. As shown in Figure 7, which presents the temporal evolution of energy densities in particles and fields for run C, in our simulations the initial plasma filamentation is accompanied by electron heating at the expense of the beam. However, the heating of the electrons saturates at  $t \approx 7\gamma_{max}^{-1}$ , when the nonresonant modes start to emerge. During the subsequent evolution, beam energy is transferred with approximately the same rate into the magnetic field and ambient ions, while the electrons experience only moderate further heating. This process of the energy transfer saturates when the turbulent magnetic field reaches its maximum energy density and starts to dissipate. The nonlinear evolution of nonresonant modes in a system containing relativistic ion beams thus proceeds in qualitatively the same way as for nonrelativistic beams.

If the cosmic-ray ion beam is represented by a constant external current, the energy conservation between the beam to the ambient medium is violated. As shown in Figure 6 (dashed lines), the saturation of the magnetic field growth still comes about by the disappearance of the ion beam-ambient plasma relative motion, at which the return current is provided without a drift of the plasma electrons relative to the plasma ions, but now the ambient ions and electrons must assume the constant cosmic-ray beam bulk velocity. This implies that energy is continuously pumped into the system, and therefore energy conservation becomes severely violated in the nonlinear stage. Thus the validity of simulations that assume a constant cosmic-ray current is limited to the early phases in the evolution of the system.

Figure 8 shows the phase-space distributions of the cosmic-ray beam and the ambient ions at  $t\gamma_{max} = 0, 7, 14,$  and  $19$  for run C. The early stage of the system evolution ( $t\gamma_{max} \lesssim 7$ ) is dominated by the Buneman instability modes between the ion beam and ambient electrons. The electrostatic fields associated with this mode heat up electrons (Fig. 7) and significantly stretch the beam ions distribution along the beam propagation direction. At the same time the cosmic-ray beam is heated in the transverse direction due to filamentation modes. The ambient ions remain unaffected by the Buneman mode<sup>1</sup> and become only moderately heated in this stage. The stretching of the beam ions distribution gradually saturates at  $t\gamma_{max} \sim 7$ , by which time the nonresonant modes have set in and started to strongly backreact on the system.

During the subsequent evolution the beam momentum becomes quickly randomized in direction. This randomization is the combined effect of the pinching of ion-beam filaments and pitch-angle scattering of the beam particles. The latter process becomes more important in the highly nonlinear phase ( $t\gamma_{max} \gtrsim 10$ ; compare Fig. 5h), during which the filaments start to get disrupted. At the same time the ion beam slows down in bulk, and

by  $t\gamma_{max} \sim 19$  the evolution saturates when the ion beam particles have been efficiently pitch-angle scattered around a mean (bulk) momentum of  $\sim -3.8m_i c$ .

The randomization of beam momentum through pitch-angle scattering was previously reported for nonrelativistic beams in conditions allowing for an efficient magnetic field amplification through nonresonant modes (Winske & Leroy 1984). Here we have demonstrated that these modes can also provide efficient scattering for relativistic beams.

We can estimate the scattering mean free path from the time evolution of the phase-space distribution of the ion beam, a few snapshots of which are shown in Figure 8. Between  $t\gamma_{max} = 10$  and  $t\gamma_{max} = 14$  the scattering mean free path in simulation run C is

$$\lambda_{\text{mfp}} \approx 5000 \Delta. \quad (3)$$

At the same time, the rms amplitude of the turbulent magnetic field increases by more than 250%, from about  $B_{\parallel 0}$  to  $3.5 B_{\parallel 0}$ . Using the mean of the two numbers, we obtain for the Bohm mean free path

$$\lambda_{\text{Bohm}} \approx 3000 \Delta \quad (4)$$

Given the uncertainty in the estimate arising from the substantial variation in the magnetic-field amplitude, about a factor 2, we conclude that the observed scattering mean free path, and therefore the spatial diffusion coefficient, for mildly relativistic beams are entirely compatible with Bohm diffusion.

The estimate of the scattering mean free path can also be made for ultrarelativistic beams based on run B. However, by the time our simulation ends the CR beam is only partially pitch-angle scattered up to an angle  $\sim \pi/6$ . Nevertheless, a rough estimate shows that  $\lambda_{\text{mfp}}$  is again within the factor of a few comparable to  $\lambda_{\text{Bohm}}$ .

## 5. DISCUSSION AND CONCLUSIONS

We have studied the interaction of a cold, relativistic ion beam penetrating a cold plasma composed of electrons and ions. We have presented 2.5D PIC simulations, complemented with a linear analysis of the dispersion relation for linear waves with arbitrary orientation of  $\vec{k}$ , for parameters that permit the growth of nonresonant, purely-magnetic parallel modes (Reville et al. 2006). Our research is relevant for the understanding of the structure of, and particle acceleration at, shocks in SNR, GRB, and AGN, for which radiation modeling suggests that the magnetic field near the shock is strongly amplified.

We observe a close competition of the nonresonant mode with the filamentation instability and Buneman modes, which is also evident in the linear dispersion relation. The specific choice of parameters determines which of the three modes of instability dominates. In some cases filamentation is initially important and modifies the later evolution of the parallel nonresonant mode. In all cases we find that a representation of the ion beam by a constant current, as is routinely done in MHD studies, is suboptimal, because it suppresses part of the nonlinear response of the system, delays the saturation processes, and leads to a significant overestimate of the final magnetic-field amplitude.

As in the case of drifting cosmic rays (Niemiec et al. 2008; Stroman et al. 2009) and nonrelativistic beams

<sup>1</sup> The phase velocity of the Buneman wave mode between cosmic-ray ion beam and electrons is  $\sim v_{CR}$  in the ambient ions rest frame. Thus the associated electrostatic fields are seen by the ambient ions as a high-frequency oscillations.

(Winske & Leroy 1984), the saturation of the magnetic-field growth proceeds via bulk acceleration. For mildly- and ultra-relativistic beams, the instability saturates at field amplitudes a few times larger than the homogeneous magnetic field. These results match our recent studies of nonrelativistically drifting cosmic-rays upstream of SNR shocks which also indicated only a moderate magnetic-field amplification by nonresonant instabilities.

We have demonstrated that the magnetic field amplified via nonresonant interactions between the CR beam and the plasma can efficiently scatter cosmic rays even for moderate field amplification levels. The scattering mean free path is compatible with Bohm diffusion. Sub-Bohm diffusion was observed in Monte-Carlo simulations of particle transport in the nonlinear turbulent magnetic field generated in the nonresonant instability by Reville et al. (2008). In that work, parallel and perpendicular diffusion coefficients were calculated by probing the spatial displacement of test particles in a static snapshot of the amplified magnetic field that resulted from MHD simulations of the instability. Here we estimate the isotropic spatial diffusion coefficient by probing the evolution of the angular distribution of particles in the self-excited, non-stationary (growing) turbulence whose typical wavelength is at least a factor of a few smaller than the gyro-radii of cosmic rays.

In the application to nonrelativistic shocks in SNRs, strong ( $\delta B/B_0 \gg 1$ ) quasi-isotropic magnetic turbulence would be compressed by the shock, thus turning into quasi-two-dimensional turbulence in the downstream region. Radio polarimetry suggests that the magnetic field immediately behind the shock is preferentially oriented along the shock normal (Stroman & Pohl 2009), which is at odds with the above expectation, if the turbulent field is not quickly damped to an amplitude  $\lesssim B_{||0}$  (Pohl et al. 2005).

In the application to relativistic shocks in AGN and GRBs, Monte-Carlo studies of the first-order Fermi acceleration have shown that the process can operate only for quasi-parallel subluminal shocks, provided that strong, short-wave magnetic turbulence exists upstream of the shock (Niemić et al. 2006). Our results show that the turbulence self-generated by the accelerated particles streaming in the shock precursor may provide scattering sufficient to randomize CR momenta. However, it is not clear how the strong quasi-isotropic magnetic turbulence in the upstream region influences the particle acceleration at the shock (but see Couch et al. (2008)).

Finally, our simulations show that the saturation of instabilities operating upstream may limit the magnetic amplitude to moderate levels. If very strong magnetic field is required by radiation modeling, it may therefore be generated at the shock itself or in the immediate downstream region.

JN and MP are grateful for the hospitality of Kavli Institute for Theoretical Physics, Santa Barbara, where this work has been completed. JN acknowledges helpful discussions with Mark Dieckmann and Luis Silva. The work of JN is supported by MNI SW research project N N203 393034, and The Foundation for Polish Science through the HOMING program, which is supported by a grant from Iceland, Liechtenstein, and Norway through the EEA Financial Mechanism. Simulations were partly performed at the Columbia facility at the NASA Advanced Supercomputing (NAS). This research was also supported in part by the National Science Foundation under Grant No. PHY05-51164 and through TeraGrid resources provided by the National Center for Supercomputing Applications (NCSA) under project PHY070013N.

## REFERENCES

- Bell, A.R. 2004, MNRAS, 353, 550  
 Bell, A.R. 2005, MNRAS, 358, 181  
 Bell, A.R., Lucek, S.G. 2001, MNRAS, 321, 433  
 Bret, A. 2009, ApJ, 699, 990  
 Buneman, O. 1993, in *Computer Space Plasma Physics: Simulation Techniques and Software*, Eds.: Matsumoto & Omura, Tokyo: Terra, p.67  
 Couch, S., Milosavljević, M., & Nakar, E. 2008, ApJ, 688, 462  
 Dieckmann, M. E., Bret, A., & Shukla, P. K. 2007, Plasma Phys. Control. Fusion, 49, 1989  
 Giacalone J., Jokipii, J.R. 2007, ApJ, 663, L41  
 Lemoine, M., Pelletier, G., & Revenu, B. 2006, ApJ, 645, L129  
 Li, Z., Waxman, E. 2006, ApJ, 651, 328  
 Malkov, M.A., Diamond, P.H. 2001, Phys. Plasmas 8 (5), 2401  
 Medvedev, M., & Zakutnyaya, O. 2009, ApJ, 696, 2269  
 Mészáros, P. 2002, ARA&A, 40, 137  
 Milosavljević, M., & Nakar, E. 2006, ApJ, 651, 979  
 Niemić, J., Ostrowski, M. 2006, ApJ, 641, 984  
 Niemić, J., Ostrowski, M., & Pohl, M. 2006, ApJ, 650, 1020  
 Niemić, J., Pohl, M., Stroman, T., & Nishikawa, K.-I. 2008, ApJ, 684, 1174  
 Ohira, Y., Reville, B., Kirk, J. G., & Takahara, F. 2009, ApJ, 698, 445  
 Pohl, M., Yan, H., Lazarian, A. 2005, ApJL 626, 101  
 Pohl, M., Lerche, I., Schlickeiser, R. 2002, A&A, 383, 309  
 Pohl, M., Schlickeiser, R. 2000, A&A, 354, 395  
 Reville, B., Kirk, J. G., & Duffy, P. 2006, Plasma Phys. Control Fusion, 48, 1741  
 Reville, B., O’Sullivan, S., Duffy, P., & Kirk, J. G. 2008, MNRAS, 386, 509  
 Reynolds, S.P. 2008, ARA&A, 46, 89  
 Riquelme, M., & Spitkovsky, A. 2009, ApJ, 694, 626  
 Sironi, L., & Spitkovsky, A. 2009, ApJ, 698, 1523  
 Spitkovsky, A. 2008a, ApJ, 673, L39  
 Spitkovsky, A. 2008b, ApJ, 682, L5  
 Stroman, W., & Pohl, M. 2009, ApJ, 696, 1864  
 Stroman, T., Pohl, M., Niemić, J. 2009, ApJ, 706, 38  
 Winske, D., Leroy, M.M. 1984, JGR, 89, 2673  
 Zirakashvili, V.N., Ptuskin, V.S. 2008, ApJ, 678, 939  
 Zirakashvili, V.N., Ptuskin, V.S., & Voelk, H.J. 2008, ApJ, 678, 255

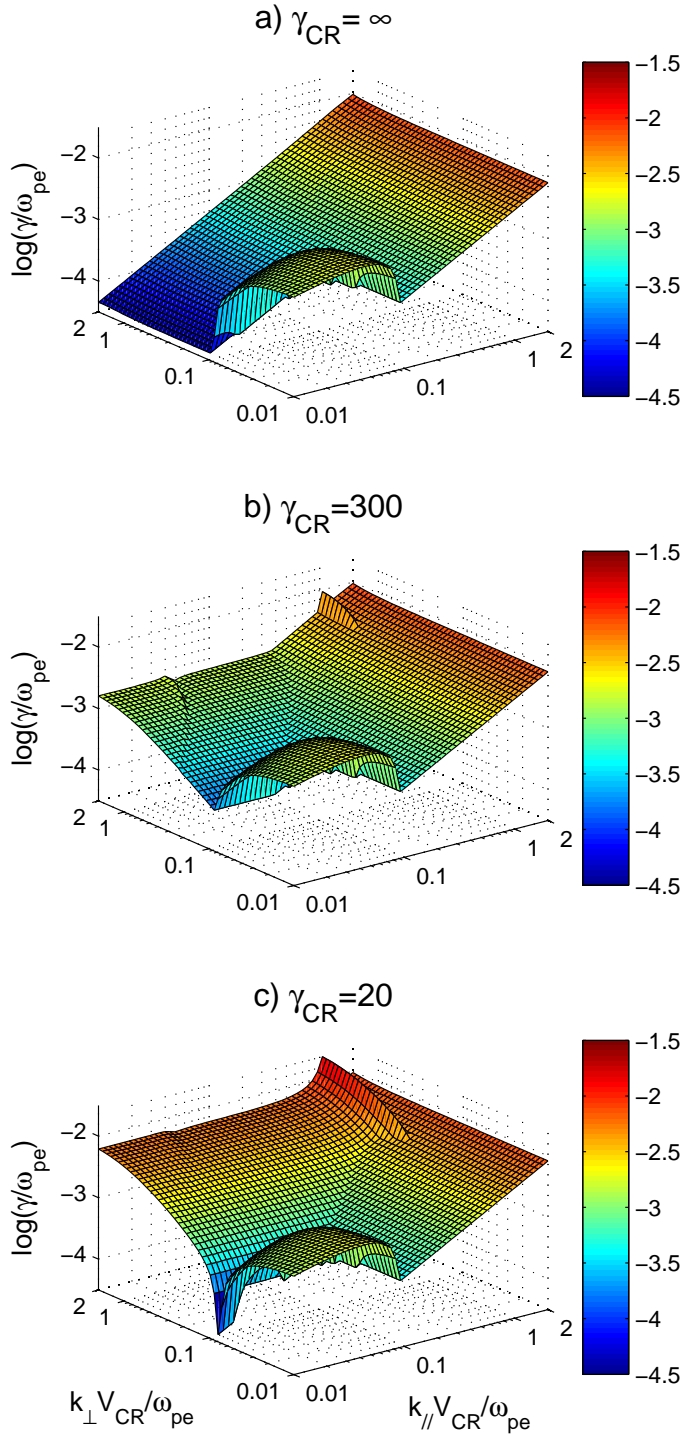


FIG. 1.— Linear growth rate  $\gamma$  in units of the electron plasma frequency,  $\omega_{pe}$ , as function of the flow-aligned and perpendicular ( $k_{\parallel}$  and  $k_{\perp}$ ) wavevectors for the parameters used in simulations A, B, and C (see Table 1). For a given  $\vec{k}$ , the growth rate of the most unstable mode is plotted. The figures show the modes whose wavelengths are well contained in the simulation box.

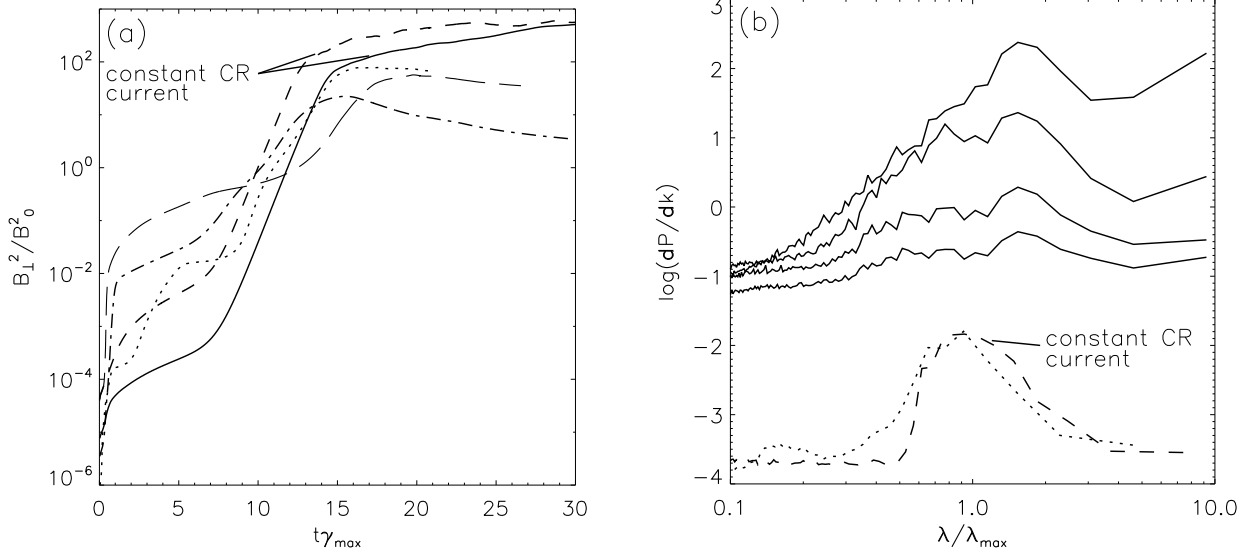


FIG. 2.— Temporal evolution of the energy density in the transverse magnetic field component, normalized to the homogeneous field strength (a). Time is dimensionless in units of the theoretically predicted inverse growth rate of the nonresonant mode,  $\gamma_{max}^{-1}$ . Simulations with constant cosmic-ray current are presented with the solid line for a plasma Alfvén velocity  $v_A = c/20$  (run A), and the dashed line for  $v_A = c/50$  (run D). The effects of cosmic-ray backreaction are shown for the case of  $v_A = c/20$  and the beam Lorentz factor  $\gamma_{CR} = 300$  (run B; dotted) and  $\gamma_{CR} = 20$  (run C; dashdotted), and for  $v_A = c/50$  and  $\gamma_{CR} = 20$  (run E; long dashed). Fourier spectra of the perpendicular magnetic-field component,  $B_z$ , in wavelengths along the beam direction for the case with  $v_A = c/20$  (runs A-C) (b). The parallel mode is expected at the wavelength  $\lambda_{max}$ . The dashed line shows results for a constant cosmic-ray current (run A), and the dotted line for a faster beam with  $\gamma_{CR} = 300$  (run B; spectrum shifted for presentation clarity) at the initial stage of the turbulence growth,  $t\gamma_{max} = 7$  and 9, respectively. Note the single peak structure centered on  $\lambda_{max}$ . The solid lines show the temporal evolution of the spectra for  $\gamma_{CR} = 20$  (run C) during the linear stage ( $t\gamma_{max} = 6, 7, 9, 11$ , from bottom to top). The magnetic turbulence appears in a broad range of wavelengths.

TABLE 1  
SIMULATION PARAMETERS AND RESULTS

Run	Grid ( $\lambda_{max}^2$ )	$t^{max}$ ( $\gamma_{max}^{-1}$ )	$N_i/N_{CR}$	$\gamma_{CR}$	$v_A$ (c)	$\gamma/\gamma_{max}$	$\delta B_{\perp}^{max}/B_{\parallel 0}$
A	$7.4 \times 5.7$	32.7	50	$\infty$	1/20	0.83	24.0
B	$4.6 \times 3.3$	21.0	50	300	1/20	0.94	8.9
C	$10.2 \times 7.4$	31.2	50	20	1/20	0.43	4.7
D	$7.4 \times 5.7$	30.2	125	$\infty$	1/50	0.79	24.0
E	$10.2 \times 7.4$	26.7	125	20	1/50	0.4	7.5

NOTE. — Parameters and selected results of the simulation runs described in this paper. Listed are: the system size in units of  $\lambda_{max}^2$ , the run duration  $t^{max}$  in units of  $\gamma_{max}^{-1}$ , the density ratio of ambient and beam ions, beam Lorentz factor, the Alfvén velocity in units of the speed of light  $c$ , the measured growth rate  $\gamma$  of the nonresonant modes in units of  $\gamma_{max}$ , and the maximum amplitude of the perpendicular magnetic field perturbations  $\delta B_{\perp}^{max}$  relative to the homogeneous magnetic field. The other parameters assumed in the simulations are: the electron skindepth  $\lambda_{se} = 4\Delta$ , the ion skindepth  $\lambda_{si} \simeq 18\Delta$ ,  $\lambda_{max} = 562\Delta$ ,  $\gamma_{max}/\Omega_i = 0.2$ , and the ion-electron mass ratio  $m_i/m_e = 20$ . The runs assuming a constant cosmic-ray current are marked with  $\gamma_{CR} = \infty$ . The growth rate  $\gamma$  is provided for time periods in which nonresonant parallel modes show up in the plasma. The amplitudes of the field turbulence for runs with constant cosmic-ray current (A and D) represent the unsaturated values at the end of these simulations.

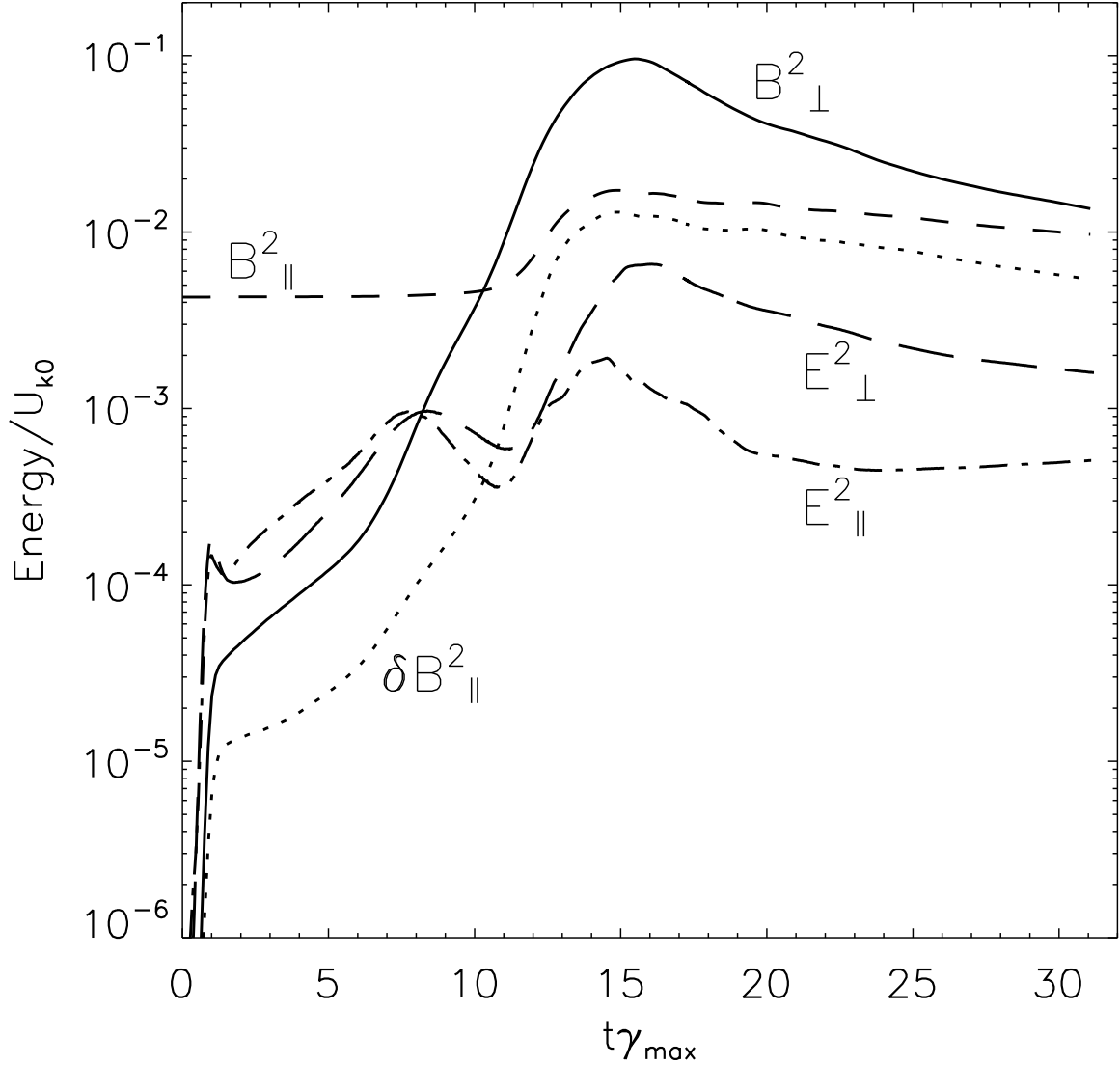


FIG. 3.— Temporal evolution of the average energy density in electromagnetic fields, normalized to the initial total kinetic energy in the system,  $U_{k0}$ , for the run with  $\gamma_{CR} = 20$  and  $v_A = c/20$  (run C; compare Fig. 2b). Here  $B_{\perp}^2$  and  $E_{\perp}^2$  indicate the magnetic and electric energy densities in the transverse components, i.e.,  $(B_y^2 + B_z^2)/(2\mu_0)$  and correspondingly for the electric field. The quantities  $B_{\parallel}^2$ ,  $\delta B_{\parallel}^2$ , and  $E_{\parallel}^2$  are defined analogously, but  $\delta B_{\parallel}^2$  refers to the turbulent component only.

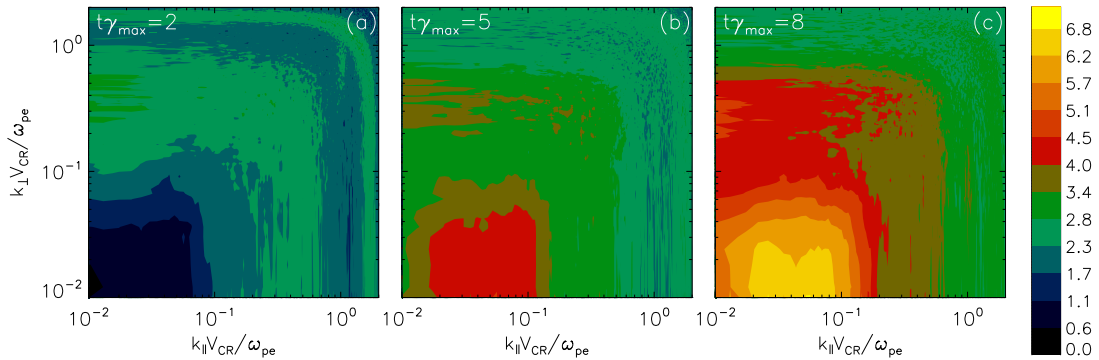


FIG. 4.— Fourier power spectra  $[\log_{10}(dP/d\lambda)]$  of the perpendicular magnetic-field component  $B_z$  in the run with  $\gamma_{CR} = 20$  and  $v_A = c/20$  (run C) for  $t = 2, 5$ , and  $8\gamma_{max}^{-1}$  in two-dimensional reduced wavevector space  $(Z_{\parallel}, Z_{\perp})$ . The wavevector range is chosen to facilitate a direct comparison with analytically predicted dispersion relation shown in Fig. 1.

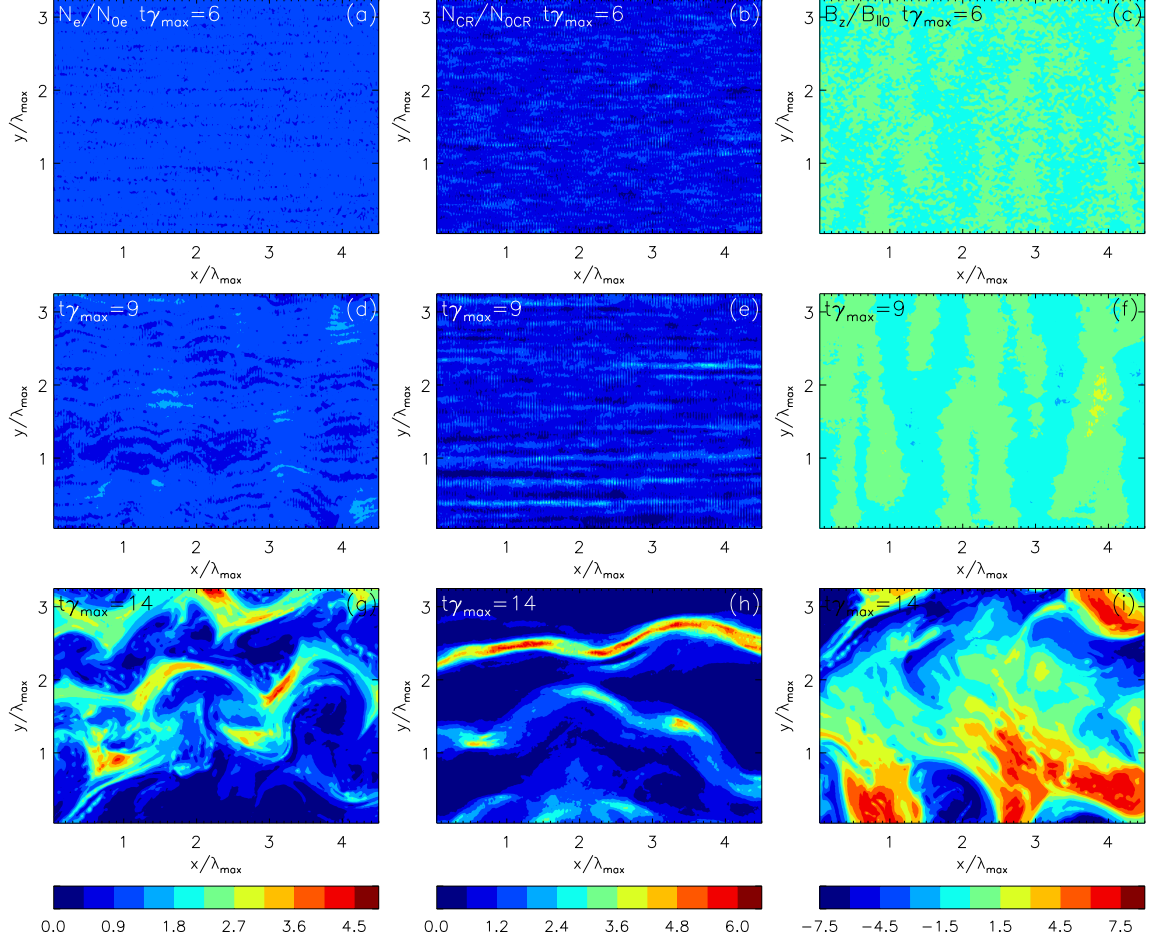


FIG. 5.— Snapshots of the time evolution of the ambient electron density (a, d, g), cosmic-ray ion density (b, e, h), and the  $B_z$  field amplitude (c, f, i) for run C at  $t\gamma_{\max} = 6$  (top), 9 (middle), and 14 (bottom). Electron and ion beam densities are normalized to their respective initial values. The magnetic field  $B_z$  is normalized to the amplitude of the homogeneous field,  $B_{||0}$ . The spatial scales are provided in units of  $\lambda_{\max}$  and only a small portion of the simulation box ( $(L_x, L_y) = (10.2\lambda_{\max}, 7.4\lambda_{\max})$ ) is shown.

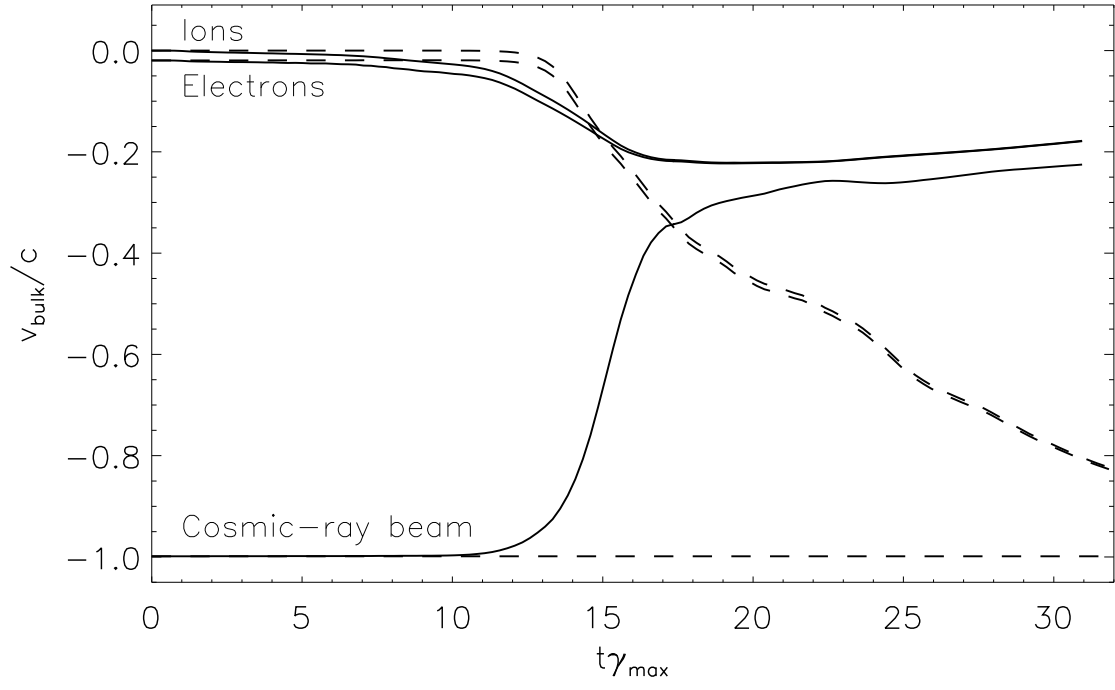


FIG. 6.— Temporal evolution of the bulk (average) velocity of all particle species for run A (dashed lines) and run C (solid lines).

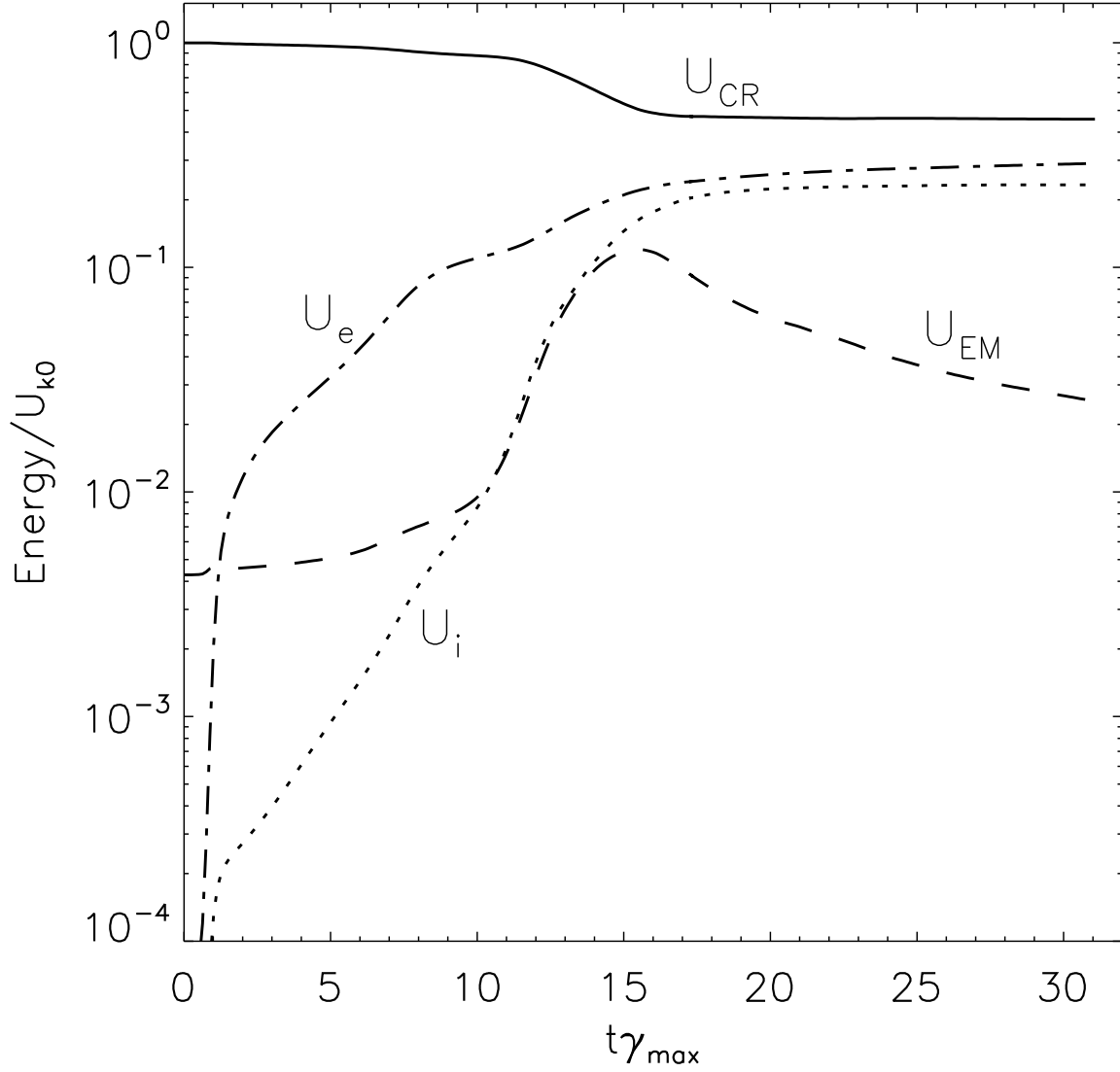


FIG. 7.— Temporal evolution of the average energy density in cosmic-ray beam ions,  $U_{CR}$ , ambient electrons,  $U_e$ , and ions,  $U_i$ , and the volume-averaged electromagnetic energy density,  $U_{EM} = \langle (B_x^2 + B_y^2 + B_z^2)/2\mu_0 + (E_x^2 + E_y^2 + E_z^2)/2 \rangle$ , for run C. All quantities are normalized to the initial total kinetic energy in the system,  $U_{k0}$ .

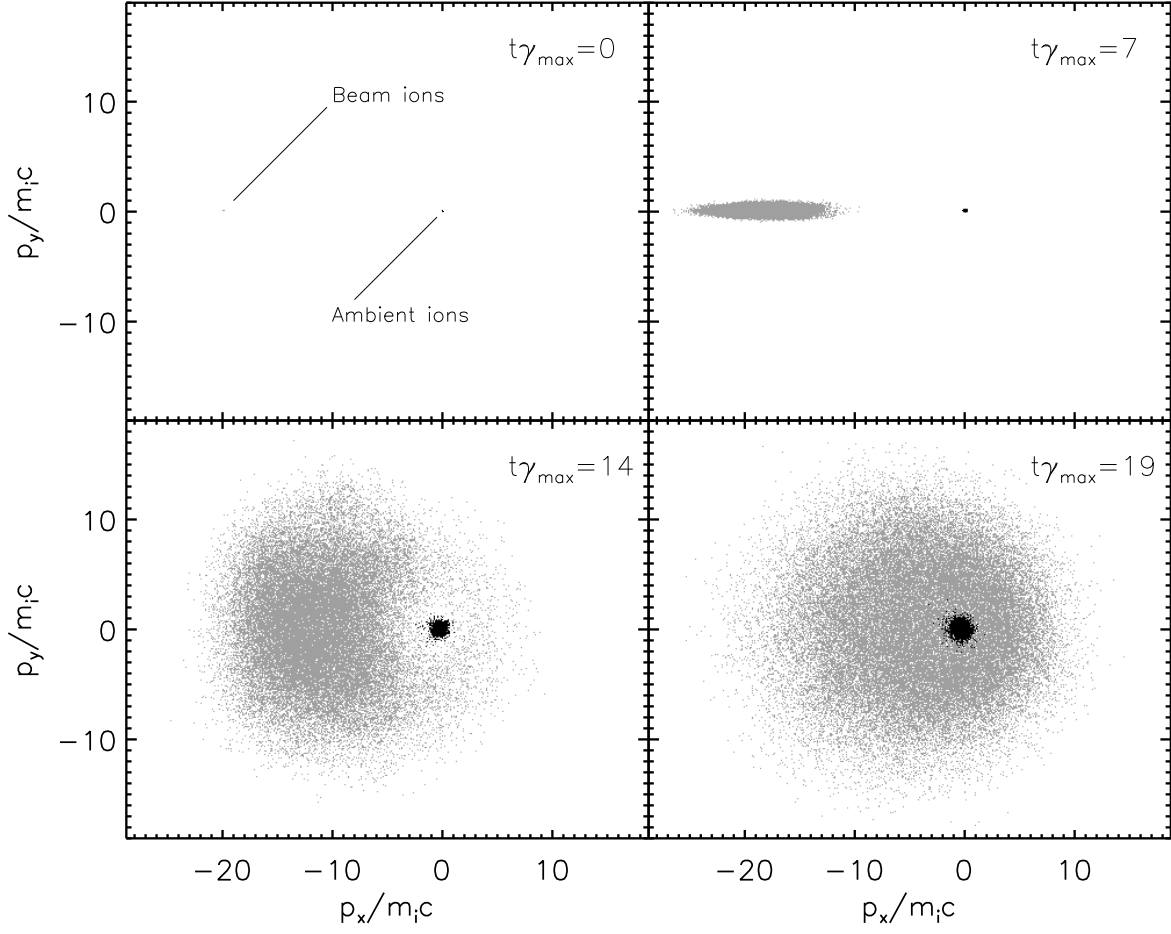


FIG. 8.— Phase-space distributions of the ions in the cosmic-ray beam (gray) and the ambient plasma (black) at  $t\gamma_{max} = 0, 7, 14$ , and  $19$  for the run with  $\gamma_{CR} = 20$  and  $v_A = c/20$  (run C).